SEU characterization of commercial and custom-designed SRAMs based on 90 nm technology and below

Andrea Coronetti, Matteo Cecchetto, Jialei Wang, Maris Tali, Pablo Fernandez Martinez, Maria Kastriotou, Athina Papadopoulou, Kacper Bilko, Florent Castellani, Mario Sacristan, Rubén García Alía, Carlo Cazzaniga, Yolanda Morilla, Pedro Martìn-Holgado, Marc-Jan van Goethem, Harry Kiewiet, Emil van der Graaf, Sytze Brandenburg, Wojtek Hajdas, Laura Sinkunaite, Miroslaw Marszalek, Heikki Kettunen, Mikko Rossi, Jukka Jaatinen, Arto Javanainen, Marie-Helene Moscatello, Anthony Dubois, Salvatore Fiore, Giulia Bazzano, Christopher Frost, Manon Letiche, Wilfrid Farabolini, Antonio Gilardi, Roberto Corsini, and Helmut Puchner

***Abstract*—The R2E project at CERN has tested a few commercial SRAMs and a custom-designed SRAM, whose data are complementary to various scientific publications. The experimental data include low- and high-energy protons, heavy ions, thermal, intermediate- and high-energy neutrons, high-energy electrons and high-energy pions.**

***Index Terms*—COTS, low-energy protons, high-energy protons, heavy ions, neutrons, electrons, pions, SEU, cross section, SRAM.**

I. Introduction

The Radiation to Electronics (R2E) project at the European Organization for Nuclear Research (CERN) has conducted several Single Event Upset (SEU) cross section characterizations of Static Random Access Memories (SRAM). These may be selected for the future versions of the RadMon [1], which is used to measure the radiation levels in the CERN accelerator complex and could be used also in other European facilities, or even embarked on cubesat missions for similar purposes.

The SRAMs under analysis have been tested in several European facilities providing a wide range of particles and energies. The list includes: standard- and high-energy heavy ions, low- and high-energy protons, thermal, intermediate- and high-energy neutrons, high-energy electrons and high-energy pions.

This study has received funding from the European Union's Horizon 2020 research and innovation programme under the MSC grant agreement no. 721624 and in part by the European Space Agency (ESA/ESTEC) at the University of Jyväskylä under Contract 4000124504/18/NL/KML/zk.

Andrea Coronetti (andrea.coronetti@cern.ch) is with CERN, CH-1211 Geneva 23, Switzerland, and with the Department of Physics, University of Jyväskylä, 40014 Jyväskylä, Finland.

Matteo Cecchetto, Maris Tali, Pablo Fernandez Martinez, Maria Kastriotou, Athina Papadopoulou, Kacper Bilko, Mario Sacristan, Rubén García Alía, Wilfrid Farabolini, Antonio Gilardi and Roberto Corsini are with CERN, CH-1211 Geneva 23, Switzerland. Antonio Gilardi is also with Università Degli Studi Di Napoli Federico II, 80138, Napoli, Italy.

Jialei Wang is with KU Leuven, Department of Electrical Engineering (ESAT), 2440 Geel, Belgium.

Florent Castellani is with ISAE Supaero, 31055 Toulouse, France.

Carlo Cazzaniga and Christopher Frost are with Science and Technology Facilities Council, OX11 0QX Didcot, UK.

Yolanda Morilla and Pedro Martin-Holgado are with Centro Nacional de Aceleradores, 41092 Seville, Spain.

Marc-Jan van Goethem, Harry Kiewiet, Emil van der Graaf and Sytze Brandenburg are with KVI-CART, 9747 AA Groningen, The Netherlands.

Wojtek Hajdas, Laura Sinkunaite and Miroslaw Marszalek are with PSI, Forschungsstrasse 111, 5232 Villigen, Switzerland.

Heikki Kettunen, Mikko Rossi, Jukka Jaatinen and Arto Javanainen are with Department of Physics, University of Jyväskylä, 40014 Jyväskylä, Finland. Arto Javanainen is also with the Electrical Engineering and Computer Science Department, Vanderbilt University, Nashville, TN 37235 USA.

Marie-Helene Moscatello and Anthony Dubois are with Grand Accelerateur National de Ions Lourdes, Boulevar Henri Becquerel, 14076 Caen Cedex 5, France.

Salvatore Fiore and Giulia Bazzano are with ENEA Centro Ricerche Frascati, Via Enrico Fermi, 45, 00044 Frascati, Italy.

Manon Letiche is with Institute Laue Langevin, 71 Avenue des Martyrs, 38000 Grenoble, France.

Helmut Puchner is with Cypress Semiconductors, Aerospace and Defence Division, San Jose, CA, 95134 USA.

II. Devices

The first SRAM is a prototype developed by one of the authors of this paper and taped out to TSMC 65-nm technology. From now on this SRAM will be referenced as RADSAGA 65-nm SRAM. This SRAM has a limited throughput of 32 kbits in its current prototype version and was produced in one single lot. The SRAM is also characterized by having a tunable core voltage in the 0.3-1.2 V range. This feature allows tuning radiation sensitivity with cross sections varying of several orders of magnitude for certain particles.

The other four SRAMs are commercially available and the main information about them are available in Table I.

Note that the Cypress 65-nm SRAM has an embedded Error Correction Code (ECC). This feature makes the SRAM less sensitive to radiation-induced SEUs. In order to use it as a detector, the ECC was disabled by firmware implementation in the Field-Programmable Gate Array (FPGA) interfacing the SRAM for read/write operations. The nominal voltage of the SRAMs is in the 2.4-3.6 V range. The ISSI SRAM data retention voltage is as low as 0.75 V. This feature has only been used in the thermal neutron test. The Cypress 65-nm SRAM also embeds an internal voltage regulator that does not allow voltage reduction.

The RADSAGA 65-nm SRAM is manufactured without plastic package. The ISSI and the three Cypress SRAMs have a plastic package. All SRAMs have been irradiated lid-off

TABLE I
MAIN FEATURES OF THE TESTED COMMERCIAL SRAMS.

Manufacturer	Reference	Datecode(s)	Technology	Array size [Mbits]
ISSI	IS61WV204816BLL-10TLI	1650	40-nm	32
Cypress	CY62167GE30-45ZXI	1731	65-nm	16
Cypress	CY62167EV30LL-45ZXA	1525, 1843	90-nm	16
Cypress	CY62157EV30LL-45ZSXI	1437, 1843	90-nm	8

only whenever the beam properties did not allow otherwise (i.e. standard-energy heavy ions, low-energy protons and high-energy electrons).

III. EXPERIMENTS

This section shortly describes the facilities where the SRAMs have been irradiated.

Concerning test conditions, the SRAMs have always been irradiated at room temperature. The RADSAGA 65-nm SRAM was irradiated statically. Data were written as all '1'. The four commercial SRAMs were irradiated either statically or dynamically. A checkerboard pattern was always used for all of them.

A. CNA

The Centro Nacional de Aceleradores (CNA) in Seville, Spain, can provide low-energy protons in the 0.5-5.9 MeV range. Protons are accelerated by means of a Tandem van der Graaff linear accelerator [2]. The voltage can be tuned so that protons can be accelerated in steps of 25 keV. The irradiation is performed inside a vacuum chamber and the device can be tilted with respect to the beam.

The proton flux is measured by means of a current integrator. Such instrument can provide the proton current measurement only for fluxes which are quite high ($10^8 - 10^{12}$ p/cm^2/s). The flux is homogeneous over a 1x1 cm^2 surface. In order to reduce the flux, the beam can be swept over an 18x18 cm^2 surface.

To measure the proton flux below the limit of the current integrator, the Devices Under Test (DUT) were irradiated alongside a reverse biased Si diode. The diode returned the flux by integrating the energy deposition pulse counts. Such a system was developed by one of the authors of this paper and calibrated at CNA with an alpha source.

B. KVI-CART

The Kernfysisch Versneller Instituut (KVI) in Groningen, The Netherlands, can provide high-energy protons and high-energy heavy ions through the AGOR cyclotron [3].

Both proton and heavy ion irradiations are performed in air. For the latter a vacuum tube is installed in the beamline and the DUT is placed in front of its exit window at about 10 cm distance.

By means of the same cyclotron, protons can be accelerated at a primary energy of 190, 66.5 or 30 MeV. The energy can be degraded by means of several combinations of Aluminium slabs of different thickness. The proton flux can be adjusted in the 10^3 - 10^8 p/cm^2/s range and it can be made homogeneous over a surface that can vary from 2x2 to 10x10 cm^2. Only when using a 3x3 (or lower) cm^2 beam field size, the flux can further be increased to 10^9 p/cm^2/s.

The cyclotron can also accelerate two cocktails of ions at different primary energies. Heavy elements (Xe, Kr, Ar and Ne) can be accelerated at a primary energy of 30 MeV/u. Light elements (He, C, O, Ne) can be accelerated at a primary energy of 90 MeV/u. The ion Linear Energy Transfer (LET) is increased by air distancing and by means of several Aluminium slabs of different thickness. The LET range can thus span from 0.025 to 60 MeV/(mg/cm^2). The ion flux for heavy elements can be tuned in the 10^2 - 10^4 ions/cm^2/s range. For the lighter elements, the flux can be tuned in the 10^3 - 10^7 ions/cm^2/s range.

For all the particles the beam is characterized and measured by means of ionization chambers.

C. PSI - PIF

The Proton Irradiation Facility (PIF) is a high-energy proton facility based at the Paul Scherrer Institute (PSI) in Villigen, Switzerland.

The PROSCAN cyclotron [4] can accelerate protons up to a primary energy of 200 MeV. During the tests, primary energies of 70 MeV and 200 MeV were used and also degraded to few intermediate energies: 150, 100, 50, 30 MeV by means of copper slabs of various thicknesses. The proton flux can be as high as $5 \cdot 10^8$ p/cm^2/s for the highest primary energy and related degraded energies. The maximum flux for the 70 MeV primary energy is $2 \cdot 10^7$ p/cm^2/s, and it reduces up to a factor 5 at 30 MeV. The beam was collimated over a 5 cm diameter surface, although smaller areas are possible.

D. RADEF

The RADiation Effects Facility (RADEF) in Jyväskylä, Finland, can provide standard- and high-energy heavy ions as well as low- and high-energy protons by means of the K-130 cyclotron.

Depending on the beam energy, proton and heavy ion irradiations can be performed in vacuum or in air. For the former standard energy (9.3 MeV/u) [5] the irradiation is performed by means of a vacuum chamber. For the new 16.3 MeV/u ion cocktail, the irradiation can be done either in vacuum or in air. The LET ranges of the two cocktails are quite compatible and can cover the 1.5-60 MeV/(mg/cm^2) range. The ion flux can be adjusted in the 10^3 - $5 \cdot 10^5$ ions/cm^2/s range over a surface of up to 5x5 cm^2. For irradiation in air, the homogeneity can be kept only up to 3x3 cm^2. The ion flux is measured by means of plastic scintillators.

The cyclotron can also accelerate protons in the 0.5-55 MeV energy range. For low energy protons [6], energies can be discriminated with steps of 200 keV. Low-energy proton irradiation is performed in vacuum. For protons with energy above 10 MeV irradiation is performed in air. The proton flux can be adjusted from 10^4 - $3 \cdot 10^8$ p/cm^2/s depending on the energy. For high energy beams, the field can be made homogeneous over a 10 cm diameter, whereas for low energy proton beams only up to 5 cm.

E. GANIL

The Grand Accelerateur National des Ions Lourdes (GANIL) in Caen, France, can provide high-energy heavy ion beams at the G4 experimental hall.

Though only a single ion species at a single primary energy is available at GANIL in each test campaign the actual kinetic energy and LET of the ion can be varied over an extended range thanks to degraders. For the experiments here reported the primary ion was Xenon at 49.4 MeV/u. The degradation is performed through air distancing and insertion of Aluminium slabs of a few hundreds of μm thickness. Since a minimum distance of 70 mm from the beam exit window was necessary to operate the x-y moving table, the primary LET of the Xenon ion was 26.84 MeV/(mg/cm^2). The maximum LET was 59.07 MeV/(mg/cm^2) and it was achieve by means of a 550 μm Aluminium slab.

The ion flux can be adjusted from a few tens ions/cm^2/s to about 10^4 ions/cm^2/s. The flux is measured by converting the pulse counts on a Silicon diode. The beam has an instantaneous size of 1x4 cm^2. In the horizontal direction the beam is swept over a 40 cm distance with a 200 Hz frequency. This makes the exploitable beam spot size as large as 40x4 cm^2.

F. ENEA

The Ente Nazionale Energie Alternative (ENEA) in Frascati, Italy, hosts a complex of machines that can be used to generate intermediate-energy neutrons and intermediate- and high-energy protons for radiation to electronics testing.

The Frascati Neutron Generator (FNG) can provide 14.8 MeV or 2.5 MeV neutrons [7]. Neutrons are generated by acceleration of a deuteron beam (up to 300 keV) which collides with either a tritium target, to produce 14.8 MeV, or a deuteron target, to obtain 2.5 MeV. The neutron flux is assessed counting the alpha particles that are produced in the fusion reaction by means of a Silicon Surface barrier Detector (SSD), with an accuracy within $\pm 3\%$. The isotropic flux of 14.8 MeV and 2.5 MeV can be as high as 10^{11} n/s and 10^9 n/s, respectively. Tests were performed at a distance from the target of 2.5 cm, resulting in a flux (considering the target ageing) of up to $3 \cdot 10^8$ n/cm^2/s at 14.8 MeV and $4 \cdot 10^6$ n/cm^2/s at 2.5 MeV.

The Terapia Oncologica con Protoni-Intensity Modulated Proton Linear Accelerator for Radio Therapy (TOP-IMPLART) is a linear accelerator at ENEA with a maximum primar proton energy of 35 MeV with a spot size of 4 mm. The LINAC emits 2.7 μs long pulses with a typical repetition frequency of 25 Hz and a peak current ranging from 1 μA to 50 μA [8]. The dosimetry is performed online by means of two ionization chambers, one at the accelerator exit and the other 15 cm before the DUT. Irradiation is performed in air and a lead scattering foil is used to obtain a large enough spot size and homogeneity [9]. This way, a 29.0 MeV beam is obtained at the test position with homogeneity of $\pm 10\%$ on a 60 mm diameter spot and flux up to $5 \cdot 10^7$ p/cm^2/s. With an additional 5 mm plexiglass degrader the energy of 18.6 MeV is obtained with a flux up to $7 \cdot 10^7$ p/cm^2/s.

G. CHIPIR

ChipIr is the most important facility for irradiation of electronics available at the ISIS neutron and muon source in Didcot, UK. It is nowadays the European neutron spallation reference facility.

Fast neutrons are released by the nuclear spallation reactions of a primary proton beam with an energy of 800 MeV with a tungsten target. The resulting fast neutron spectrum is delivered to the ChipIr facility [10], [11]. The neutron spectrum has an energetic distribution which resembles that of atmospheric neutrons with an acceleration factor which is as high as 10^9 with respect to the sea level neutron flux.

The flux provided by the facility is that of neutrons above 10 MeV and it corresponds to about $5 \cdot 10^6$ n/cm^2/s. The beam is generally delivered at the facility over a 7x7 cm^2 surface, but this size can be extended up to 40x40 cm^2 without impact on the flux. Thanks to the deep penetration of the beam, it is possible to stack and test several devices simultaneously with minimal effect on the flux.

H. ILL

The Institute Laue Langevin, located in Grenoble, France, can provide neutrons for irradiation of electronics which are released by a nuclear reactor.

The fast neutrons released by the reactor are cooled down to thermal energies (peaking at 10 meV) by means of liquid deuterium at 20 K [12]. The corresponding thermal neutron flux (at 25 meV) available at the D50 facility is of the order of 10^9 n/cm^2/s. The flux is measured with the gold foil activation technique and the target fluence can be achieved by setting up a certain irradiation time. The flux is homogeneous over a 1.5 cm^2 surface.

I. CERN - VESPER

VESPER is an electron LINAC (Linear accelerator) facility based at CERN, Geneva, Switzerland. The electrons are released by means of a laser gun and accelerated by a sequence of accelerating structures in an energy range of 55-220 MeV [13], [14].

The VESPER test station receives electrons for irradiation of devices. The beam spot size is measured with a YAG screen and it can be as low as 0.5 cm or as large as 3 cm.

The flux is tunable over few orders of magnitude. When generated by the laser gun, the electron flux can only be as low as 30 pC/pulse, i.e. about $5 \cdot 10^7$ e/cm^2/s depending on the full-width half-maximum and the pulse repetition rate. The flux can be increased up to 10 nC/pulse, i.e.

about 10^{11} e/cm^2/s when using the maximum repetition rate (10 Hz). Given the pulsed nature of the beam (electrons are delivered to the DUT in bunches, i.e., fractions of a pulse, at a 3 GHz frequency), the DUT may suffer from radiation effect artifacts (e.g. localized SEFIs) in this beam if the flux is too high. For this reason the flux was kept close to its lower end for all the various irradiations.

J. PSI - PIM1

PIM1 is an electron and pion facility based at the Paul Scherrer Institute (PSI) in Villigen, Switzerland.

Electrons and pions (with a small fraction of muons) are produced by nuclear spallation of a high-energy proton beam (590 MeV) accelerated by a cyclotron with a tungsten target. An extraction beamline can direct electrons and pions to the test position by means of a double magnet bending structure. The extracted beam is composed of electrons and pions sharing the same momentum, but having different energies. The beam concentration varies according to the momentum [15], [16]. At low momenta, the beam is almost fully composed of electrons, whereas at high momenta it is almost fully composed of pions.

Pion testing can be performed in an energy range of 50-233 MeV. Due to the beam composition, however, the maximum pion flux available also varies with the momentum/energy. Due to the high electron concentration, the flux at 50 MeV is limited to $5 \cdot 10^4$ π/cm^2/s. At 233 MeV the flux can reach up to $5 \cdot 10^6$ π/cm^2/s. The beam is homogeneous within $\pm$10% over a surface with 1 cm diameter.

IV. Results

The data are presented with error bars calculated at 95% confidence level considering the uncertainty on the fluence (10%) and on the number of events. If error bars are not visible, it is because they are smaller than the markers.

In such cases for which 0 or few events were observed the upper bound is calculated with 95% confidence according to a Poisson distribution [17].

Having two different datecodes, for the Cypress 90-nm SRAMs, the datecode for each data-point is indicated in brackets in the captions of the figures.

The RADSAGA 65 nm SRAM shows a very strong sensitivity to proton direct ionization (PDI), Fig. 1. This is moderated efficiently by voltage, to the point that at 1.2 V, the PDI peak almost disappears. Such feature makes it an interesting memory to be flown in Low-Earth Orbit (LEO) to confirm whether PDI may become the dominant contributor to the soft error rate of similar devices.

Strong PDI cross section enhancement was also found for the other two SRAMs. For the ISSI SRAM (Fig. 4), several measurements were performed. While the datecode is the same, the data refer to three different units. Remarkably, the data show different peaks, with the very maximum measured for the unit tested at RADEF. Also the breadth of the peak changes significantly.

All the memories showing a high and wide PDI peak are based on a 65-nm technology or below. The last memory (Fig. 8), based on 90-nm technology, still has a quite high peak, but this is pretty restricted to a very narrow energy range.

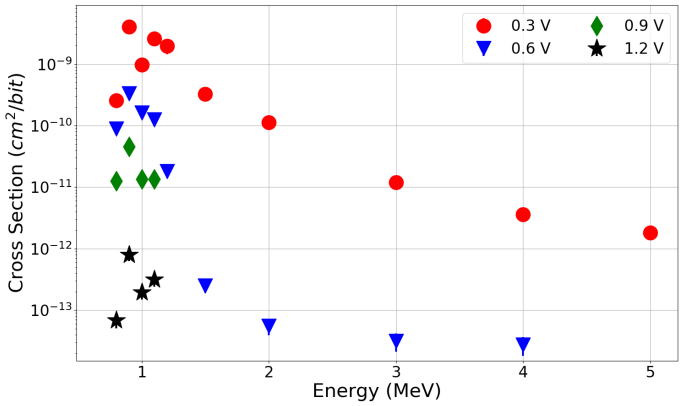

Fig. 1. Low-energy proton cross section as a function of energy and core voltage for the RADSAGA 65-nm SRAM. Data from CNA.

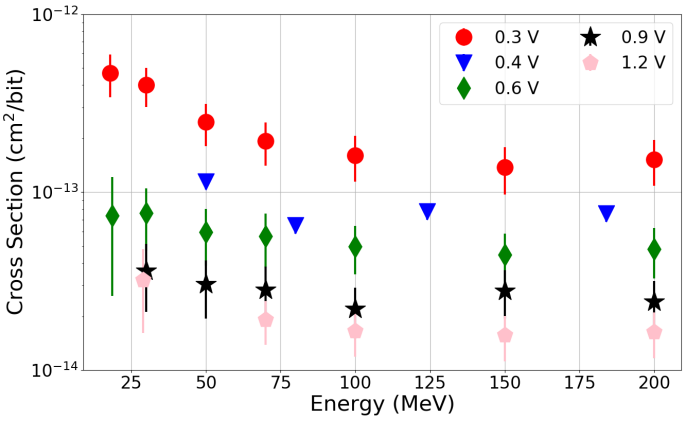

Fig. 2. High-energy proton cross section as a function of energy and core voltage for the RADSAGA 65-nm SRAM. Data from ENEA (18.5 and 29 MeV) and PSI and KVI-CART (30-200 MeV).

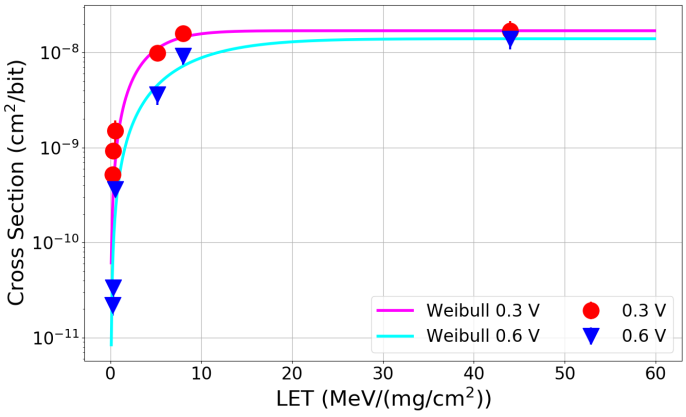

Fig. 3. Heavy ion cross section as a function of LET and core voltage for the RADSAGA 65-nm SRAM. Data from KVI-CART. Weibull parameters for 0.3 V: σ_{sat} = 1.7 $\cdot$ 10^{-8} cm^2/bit, LET_{th} = 0.07 MeV/(mg/cm^2), W = 1 MeV/(mg/cm^2), s = 2.4. Weibull parameters for 0.6 V: σ_{sat} = 1.4 $\cdot$ 10^{-8} cm^2/bit, LET_{th} = 0.07 MeV/(mg/cm^2), W = 10 MeV/(mg/cm^2), s = 1.4.

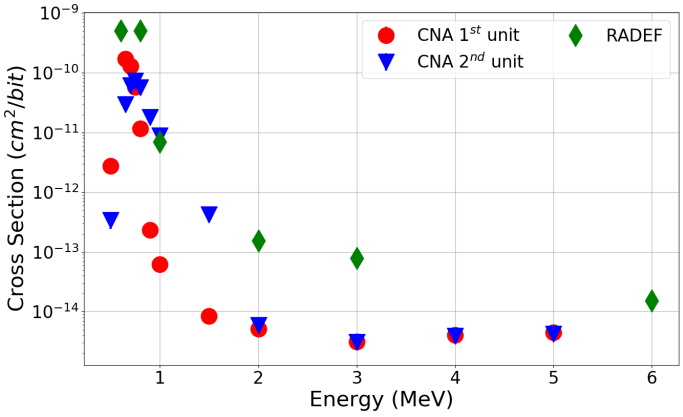

Fig. 4. Low-energy proton cross section as a function of energy for the ISSI 40-nm SRAM. Data from CNA for two units and from RADEF for another unit. All units have the same datecode.

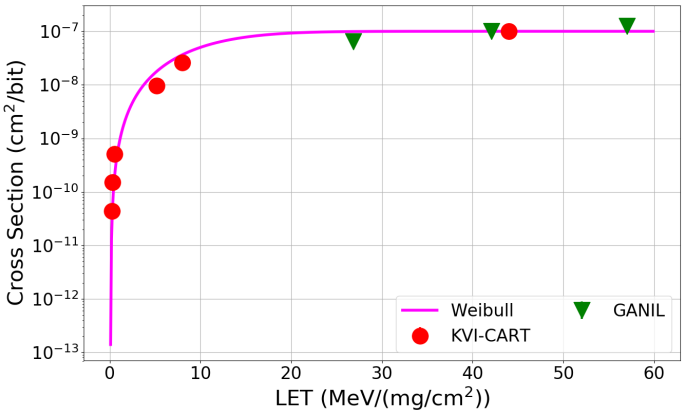

Fig. 7. Heavy ion cross section as a function of LET for the Cypress 65-nm SRAM. Data from KVI-CART and GANIL. Weibull parameters: σ_{sat} = 1 · 10^{-7} cm^2/bit, LET_{th} = 0.09 MeV/(mg/cm^2), W = 12 MeV/(mg/cm^2), s = 1.9.

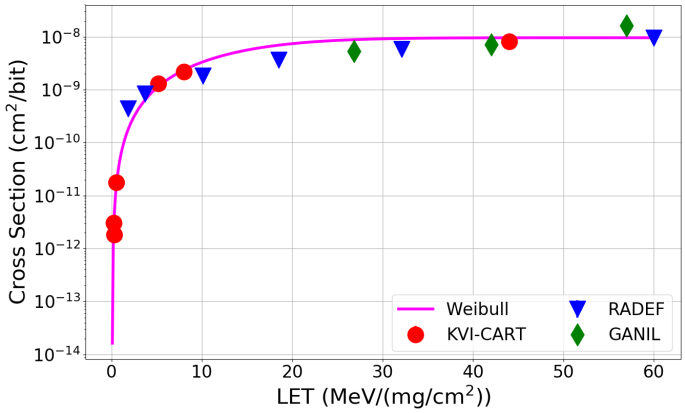

Fig. 5. Heavy ion cross section as a function of LET for the ISSI 40-nm SRAM. Data from KVI-CART, RADEF and GANIL. Weibull parameters: σ_{sat} = 9.56 · 10^{-9} cm^2/bit, LET_{th} = 0.09 MeV/(mg/cm^2), W = 16 MeV/(mg/cm^2), s = 1.8.

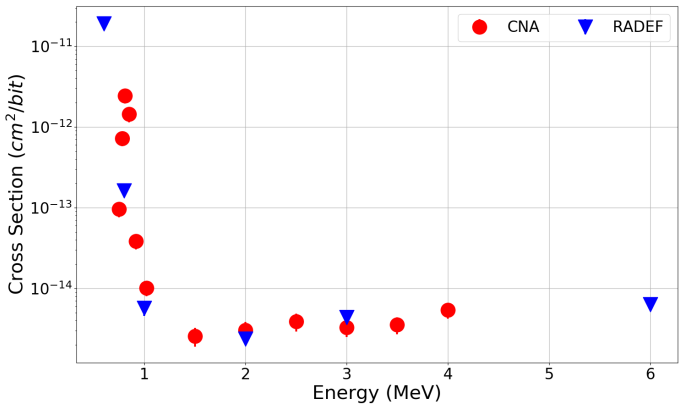

Fig. 8. Low-energy proton cross section as a function of energy for the Cypress 90-nm 16-Mbit SRAM. Data from CNA (1843) and RADEF (1525).

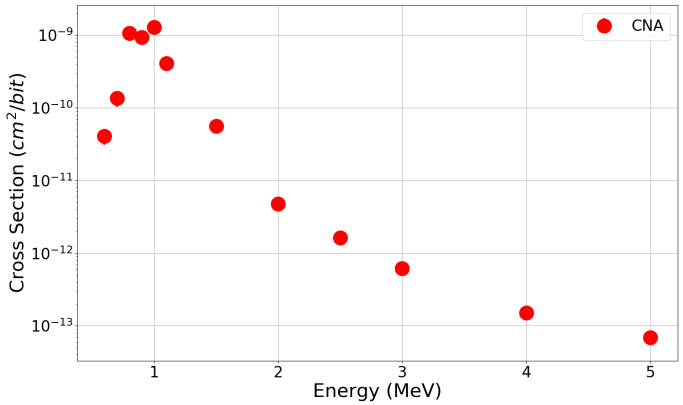

Fig. 6. Low-energy proton cross section as a function of energy for the Cypress 65-nm SRAM. Data from CNA.

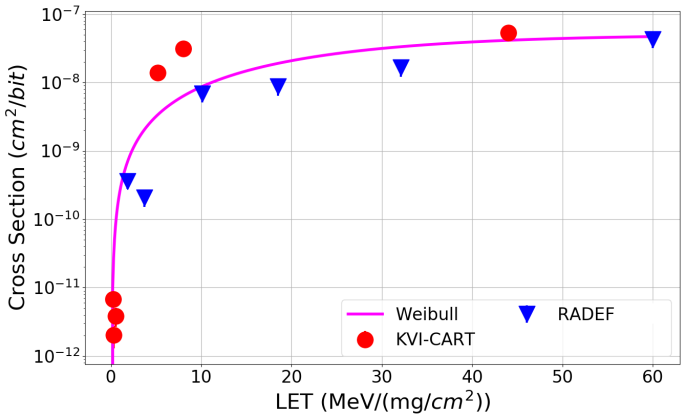

Fig. 9. Heavy ion cross section as a function of LET for the Cypress 90-nm 16-Mbit SRAM. Data from KVI-CART (1843) and RADEF (1525). Weibull parameters: $\sigma_{sat} = 5.0 \cdot 10^{-8}$ cm^2/bit, LET_{th} = 0.1 MeV/(mg/cm^2), W = 30 MeV/(mg/cm^2), s = 1.5.

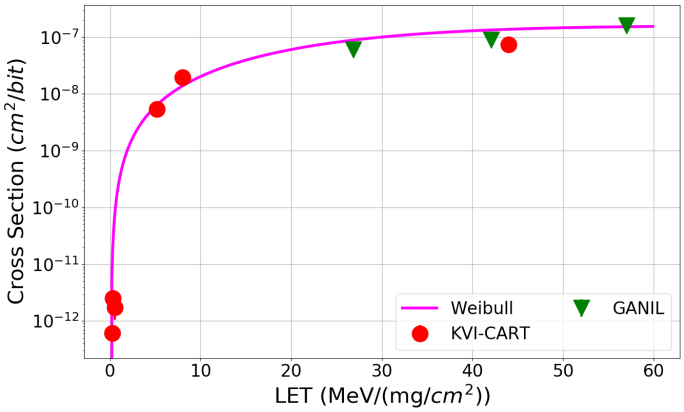

Fig. 10. Heavy ion cross section as a function of LET for the Cypress 90-nm 8-Mbit SRAM. Data from KVI-CART (1843) and GANIL (1843). Weibull parameters: $\sigma_{sat} = 1.6 \cdot 10^{-7}$ cm^2/bit, LET_{th} = 0.1 MeV/(mg/cm^2), W = 30 MeV/(mg/cm^2), s = 1.8.

REFERENCES

[1] G. Spiezia, P. Peronnard, A. Masi, M. Brugger, M. Brucoli, S. Danzeca, "A new RadMon version for the LHC and its injection lines," IEEE Trans. Nucl. Sci., vol. 61, no. 6, pp. 3424-3431, December 2014.

[2] Y. Morilla, P. Martin-Holgado, A. Romero, J.A. Labrador, B. Fernandez, "Progress of CNA to become the spanish facility for combined irradiation testing in aerospace," RADECS proceedings, 2018.

[3] E.R. van der Graaf, R.W. Ostendorf, M.J. van Goethem, H.H. Kiewiet, "AGORFIRM, the AGOR facility for irradiations of material," RADECS proceedings, 2009.

[4] W. Hajdas, F. Burri, C. Eggel, R. Harboe-Sorensen, R. de Marino, "Radiation effects testing facilities in PSI during implementation of the PROSCAN project," NSREC Radiation Effects Data Workshop, 2002.

[5] A. Virtanen, R. Harboe-Sorensen, A. Javanainen, H. Kettunen, H. Koivisto, "Upgrades for the RADEF facility," RADECS Data Workshop, 2007.

[6] H. Kettunen, V. Ferlet-Cavrois, P. Roche, M. Rossi, A. Bosser, "Low energy protons at RADEF - application to advanced eSRAMs," RADECS Data Workshop, 2014.

[7] S. Fiore, M. Angelone, S. Loreti, A. Pietropaolo, M. Pillon, "The Frascati Neutron Generator FNG: a fast neutron facility for irradiation experiments," RADECS 2018 conference proceedings.

[8] L. Picardi, A. Ampolini, G. Bazzano, E. Cisbani, F. Ghio, "Beam commissioning of the 35 MeV section in an intensity modulated proton linear accelerator for proton therapy," Phys. Rev. Accel. Beams, vol. 23, no. 020102, 2020.

[9] G. Bazzano, A. Ampollini, L. Blasi, F. Cardelli, E. Cisbani, "Dosimetric characterization of an irradiation setup for electronic components testing at the TOPIMPLART proton linear accelerator," RADECS 2019 conference proceedings.

[10] C. Cazzaniga, M. Bagatin, S. Gerardin, A. Costantino, C. Frost, "First tests of a new facility for device-level, board-level and system-level neutron irradiation of microelectronics," IEEE Trans. Emerg. Topics Comput., early access, 2018.

[11] D. Chiesa, M. Nastasi, C. Cazzaniga, M. Rebai, L. Arcidiacono et al., "Measurement of the neutron flux at spallation sources using multi-foil activation," Nucl. Intrum. Methods Phys. Res. A, Accel. Spectrom. Detect. Assoc. Equip., vol. 902, pp 14-24, 2018.

[12] M. Cecchetto, "Impact of thermal and intermediate energy neutrons on the semiconductor memories for the CERN accelerators," M.S. thesis, Dept. Inf. Eng., Padova Univ., Padua, Italy, 2017.

[13] K.N. Sjobak, E. Adli, C.A. Lindstrom, M. Bergamaschi, S. Burger et al., "Status of the CLEAR electron beam user facility at CERN," in 10th International Particle Accelerator Conference (IPAC), Melbourne, Australia, 2019.

[14] M. Tali, R. Garcia Alia, M. Brugger, V. Ferlet-Cavrois, R. Corsini et al., "High-energy electron-induced SEUs and Jovian Environment Impact," IEEE Trans. Nucl. Sci., vol. 64, no. 8, pp. 2016-2022, August 2017.

[15] W. Hajdas, L. Desorgher, K. Deiters, D. Reggiani, T. Rauber, "High energy electron radiation exposure facility at PSI," Journal of Applied Mathematics and Physics, vol. 2, pp. 910-917, August 2014.

[16] A. Coronetti, R. Garcia Alia, M. Cecchetto, W. Hajdas, D. Söderström, "The pion single event effect resonance and its impact in an accelerator environment," IEEE Trans. Nucl. Sci., vol. 67, no. 7, pp. 1606-1613, July 2020.

[17] G.M. Swift, "SEE testing lessons from Dickens, Scounting and Oz," SEE Symposium, 2006.

TABLE II
SEU CROSS-SECTIONS OF THE RADSAGA 65-NM SRAM (NEUTRONS) AND OF THE IS61WV204816BLL-10TLI (NEUTRONS, ELECTRONS AND PIONS).

Test facility	Particle	Energy [MeV]	Datecode	Voltage [V]	Cross-section [cm^2/bit]
RADSAGA					
ILL	n	$2.5 \cdot 10^{-8}$	-	0.25	$7.15 \cdot 10^{-14} \pm 2.4 \cdot 10^{-14}$
ILL	n	$2.5 \cdot 10^{-8}$	-	0.3	$4.74 \cdot 10^{-14} \pm 1.3 \cdot 10^{-14}$
ENEA	n	14.8	-	0.3	$1.59 \cdot 10^{-13} \pm 5.7 \cdot 10^{-14}$
ILL	n	$2.5 \cdot 10^{-8}$	-	0.4	$4.43 \cdot 10^{-14} \pm 1.2 \cdot 10^{-14}$
ILL	n	$2.5 \cdot 10^{-8}$	-	0.6	$3.14 \cdot 10^{-14} \pm 9.5 \cdot 10^{-15}$
ENEA	n	14.8	-	0.6	$7.50 \cdot 10^{-14} \pm 4.5 \cdot 10^{-14}$
ILL	n	$2.5 \cdot 10^{-8}$	-	0.8	$2.48 \cdot 10^{-14} \pm 8.1 \cdot 10^{-15}$
ILL	n	$2.5 \cdot 10^{-8}$	-	0.9	$1.89 \cdot 10^{-14} \pm 6.7 \cdot 10^{-15}$
ENEA	n	14.8	-	0.9	$3.84 \cdot 10^{-14} \pm 2.2 \cdot 10^{-14}$
ILL	n	$2.5 \cdot 10^{-8}$	-	1.2	$1.61 \cdot 10^{-14} \pm 6.0 \cdot 10^{-15}$
ENEA	n	14.8	-	1.2	$2.81 \cdot 10^{-14} \pm 1.8 \cdot 10^{-14}$
IS61WV204816BLL-10TLI					
ILL	n	$2.5 \cdot 10^{-8}$	1650	0.6	$1.62 \cdot 10^{-14} \pm 3.6 \cdot 10^{-15}$
ILL	n	$2.5 \cdot 10^{-8}$	1650	0.7	$7.91 \cdot 10^{-15} \pm 1.9 \cdot 10^{-15}$
ILL	n	$2.5 \cdot 10^{-8}$	1650	0.8	$6.03 \cdot 10^{-15} \pm 1.7 \cdot 10^{-15}$
ILL	n	$2.5 \cdot 10^{-8}$	1650	0.9	$5.17 \cdot 10^{-15} \pm 1.5 \cdot 10^{-15}$
ILL	n	$2.5 \cdot 10^{-8}$	1650	1	$5.26 \cdot 10^{-15} \pm 1.5 \cdot 10^{-15}$
ILL	n	$2.5 \cdot 10^{-8}$	1650	1.1	$5.02 \cdot 10^{-15} \pm 1.5 \cdot 10^{-15}$
ILL	n	$2.5 \cdot 10^{-8}$	1650	1.2	$4.56 \cdot 10^{-15} \pm 1.4 \cdot 10^{-15}$
ILL	n	$2.5 \cdot 10^{-8}$	1650	1.3	$4.92 \cdot 10^{-15} \pm 1.5 \cdot 10^{-15}$
ILL	n	$2.5 \cdot 10^{-8}$	1650	1.4	$4.66 \cdot 10^{-15} \pm 1.4 \cdot 10^{-15}$
ILL	n	$2.5 \cdot 10^{-8}$	1650	1.5	$5.89 \cdot 10^{-15} \pm 1.7 \cdot 10^{-15}$
ILL	n	$2.5 \cdot 10^{-8}$	1650	1.6	$4.80 \cdot 10^{-15} \pm 1.2 \cdot 10^{-15}$
ILL	n	$2.5 \cdot 10^{-8}$	1650	1.7	$4.48 \cdot 10^{-15} \pm 1.4 \cdot 10^{-15}$
ILL	n	$2.5 \cdot 10^{-8}$	1650	1.8	$4.40 \cdot 10^{-15} \pm 1.4 \cdot 10^{-15}$
ILL	n	$2.5 \cdot 10^{-8}$	1650	1.9	$3.76 \cdot 10^{-15} \pm 1.0 \cdot 10^{-15}$
ILL	n	$2.5 \cdot 10^{-8}$	1650	2	$3.96 \cdot 10^{-15} \pm 1.1 \cdot 10^{-15}$
ILL	n	$2.5 \cdot 10^{-8}$	1650	2.1	$3.73 \cdot 10^{-15} \pm 1.0 \cdot 10^{-15}$
ILL	n	$2.5 \cdot 10^{-8}$	1650	2.2	$3.80 \cdot 10^{-15} \pm 1.0 \cdot 10^{-15}$
ILL	n	$2.5 \cdot 10^{-8}$	1650	2.4	$4.21 \cdot 10^{-15} \pm 1.1 \cdot 10^{-15}$
ILL	n	$2.5 \cdot 10^{-8}$	1650	2.6	$4.25 \cdot 10^{-15} \pm 1.1 \cdot 10^{-15}$
ILL	n	$2.5 \cdot 10^{-8}$	1650	2.8	$3.83 \cdot 10^{-15} \pm 1.0 \cdot 10^{-15}$
ILL	n	$2.5 \cdot 10^{-8}$	1650	3	$3.89 \cdot 10^{-15} \pm 1.0 \cdot 10^{-15}$
ILL	n	$2.5 \cdot 10^{-8}$	1650	3.3	$3.16 \cdot 10^{-15} \pm 6.4 \cdot 10^{-16}$
ILL	n	$2.5 \cdot 10^{-8}$	1650	3.6	$4.11 \cdot 10^{-15} \pm 1.1 \cdot 10^{-15}$
ENEA	n	2.5	1650	3.3	$2.20 \cdot 10^{-15} \pm 5.1 \cdot 10^{-16}$
ENEA	n	14.8	1650	3.3	$9.81 \cdot 10^{-15} \pm 2.1 \cdot 10^{-15}$
CHIPIR	n	spectra	1650	3.3	$9.69 \cdot 10^{-15} \pm 2.0 \cdot 10^{-15}$
VESPER	e^-	60	1650	3.3	$1.36 \cdot 10^{-18} \pm 7.9 \cdot 10^{-19}$
VESPER	e^-	120	1650	3.3	$3.32 \cdot 10^{-18} \pm 1.6 \cdot 10^{-18}$
VESPER	e^-	200	1650	3.3	$4.74 \cdot 10^{-18} \pm 2.2 \cdot 10^{-18}$
PSI - PIM1	π^-	51	1650	3.3	$1.54 \cdot 10^{-14} \pm 6.9 \cdot 10^{-15}$
PSI - PIM1	π^-	104	1650	3.3	$3.27 \cdot 10^{-14} \pm 1.3 \cdot 10^{-14}$
PSI - PIM1	π^-	164	1650	3.3	$3.70 \cdot 10^{-14} \pm 1.5 \cdot 10^{-14}$
PSI - PIM1	π^-	233	1650	3.3	$3.14 \cdot 10^{-14} \pm 1.3 \cdot 10^{-14}$

TABLE III
SEU CROSS-SECTIONS OF THE CY62167GE30-45ZXI (NEUTRONS AND ELECTRONS), OF THE CY62167EV30LL-45ZXA (NEUTRONS, ELECTRONS AND PIONS) AND OF THE CY62157EV30LL-45ZSXI (NEUTRONS AND PIONS).

Test facility	Particle	Energy [MeV]	Datecode	Voltage [V]	Cross-section [cm^2/bit]
CY62167GE30-45ZXI					
ILL	n	$2.5 \cdot 10^{-8}$	1731	3.3	$4.91 \cdot 10^{-16} \pm 1.1 \cdot 10^{-16}$
ENEA	n	2.5	1731	3.3	$1.97 \cdot 10^{-16} \pm 9.5 \cdot 10^{-17}$
ENEA	n	14.8	1731	3.3	$4.60 \cdot 10^{-14} \pm 9.4 \cdot 10^{-15}$
VESPER	e^-	60	1731	3.3	$5.16 \cdot 10^{-17} \pm 2.9 \cdot 10^{-17}$
VESPER	e^-	120	1731	3.3	$8.46 \cdot 10^{-17} \pm 5.4 \cdot 10^{-17}$
VESPER	e^-	200	1731	3.3	$6.28 \cdot 10^{-17} \pm 4.0 \cdot 10^{-17}$
CY62167EV30LL-45ZXA					
ILL	n	$2.5 \cdot 10^{-8}$	1843	3.3	$3.88 \cdot 10^{-16} \pm 9.2 \cdot 10^{-17}$
ENEA	n	2.5	1843	3.3	$2.75 \cdot 10^{-15} \pm 9.1 \cdot 10^{-16}$
ENEA	n	14.8	1843	3.3	$2.99 \cdot 10^{-14} \pm 6.2 \cdot 10^{-15}$
CHIPIR	n	spectra	1525	3.3	$3.95 \cdot 10^{-14} \pm 8.0 \cdot 10^{-15}$
VESPER	e^-	60	1843	3.3	$1.90 \cdot 10^{-18} \pm 1.4 \cdot 10^{-18}$
VESPER	e^-	120	1843	3.3	$1.13 \cdot 10^{-17} \pm 6.0 \cdot 10^{-18}$
VESPER	e^-	200	1843	3.3	$2.83 \cdot 10^{-17} \pm 1.3 \cdot 10^{-17}$
PSI - PIM1	π^-	51	1525	3.3	$5.05 \cdot 10^{-14} \pm 2.1 \cdot 10^{-14}$
PSI - PIM1	π^-	104	1525	3.3	$1.90 \cdot 10^{-13} \pm 7.6 \cdot 10^{-14}$
PSI - PIM1	π^-	164	1525	3.3	$2.9 \cdot 10^{-13} \pm 1.2 \cdot 10^{-13}$
PSI - PIM1	π^-	233	1525	3.3	$2.20 \cdot 10^{-13} \pm 8.8 \cdot 10^{-14}$
CY62157EV30LL-45ZSXI					
ILL	n	$2.5 \cdot 10^{-8}$	1843	3.3	$5.80 \cdot 10^{-16} \pm 1.3 \cdot 10^{-16}$
ENEA	n	2.5	1843	3.3	$2.75 \cdot 10^{-15} \pm 9.1 \cdot 10^{-16}$
ENEA	n	14.8	1843	3.3	$5.06 \cdot 10^{-14} \pm 1.1 \cdot 10^{-14}$
CHIPIR	n	spectra	1437	3.3	$5.73 \cdot 10^{-14} \pm 1.3 \cdot 10^{-14}$
PSI - PIM1	π^-	51	1437	3.3	$9.21 \cdot 10^{-14} \pm 3.9 \cdot 10^{-14}$
PSI - PIM1	π^-	104	1437	3.3	$1.70 \cdot 10^{-13} \pm 6.8 \cdot 10^{-14}$
PSI - PIM1	π^-	164	1437	3.3	$1.85 \cdot 10^{-13} \pm 7.4 \cdot 10^{-14}$
PSI - PIM1	π^-	233	1437	3.3	$1.54 \cdot 10^{-13} \pm 6.2 \cdot 10^{-14}$